In Vitro Biocompatibility and Antibacterial Efficacy of a Degradable Poly(L-lactide-co-epsilon-caprolactone) Copolymer Incorporated with Silver Nanoparticles

MEGHAN E. SAMBERG,[1,2] PETER MENTE,[2] TING HE,[3] MARTIN W. KING,[3]
and NANCY A. MONTEIRO-RIVIERE[1,2,4]

[1]Center for Chemical Toxicology Research and Pharmacokinetics, North Carolina State University, Raleigh, NC, USA; [2]Joint Department of Biomedical Engineering at the University of North Carolina at Chapel Hill and North Carolina State University, Raleigh, NC, USA; [3]College of Textiles, North Carolina State University, Raleigh, NC, USA; and [4]Department of Anatomy and Physiology, Nanotechnology Innovation Center of Kansas State (NICKS), Kansas State University, Manhattan, KS, USA

Abstract—Silver nanoparticles (Ag-nps) are currently used as a natural biocide to prevent undesired bacterial growth in clothing, cosmetics and medical products. The objective of the study was to impart antibacterial properties through the incorporation of Ag-nps at increasing concentrations to electrospun degradable 50:50 poly(L-lactide-co-epsilon-caprolactone) scaffolds for skin tissue engineering applications. The biocompatibility of the scaffolds containing Ag-nps was evaluated with human epidermal keratinocytes (HEK); cell viability and proliferation were evaluated using Live/Dead and alamarBlue viability assays following 7 and 14 days of cell culture on the scaffolds. Significant decreases in cell viability and proliferation were noted for the 1.0 mg(Ag) g(scaffold)$^{-1}$ after 7 and 14 days on Ag-nps scaffolds. After 14 days, scanning electron microscopy revealed a confluent layer of HEK on the surface of the 0.0 and 0.1 mg(Ag) g(scaffold)$^{-1}$. Both 0.5 and 1.0 mg(Ag) g(scaffold)$^{-1}$ were capable of inhibiting both Gram positive and negative bacterial strains. Uniaxial tensile tests revealed a significant ($p < 0.001$) decrease in the modulus of elasticity following Ag-nps incorporation compared to control. These findings suggest that a scaffold containing between 0.5 and 1.0 mg(Ag) g(scaffold)$^{-1}$ is both biocompatible and antibacterial, and is suitable for skin tissue engineering graft scaffolds.

Keywords—Nanoparticle, Keratinocyte, Skin tissue engineering, Scaffold, Biocompatibility.

INTRODUCTION

The skin, the largest organ of the body, performs numerous vital functions, including fluid homeostasis, thermoregulation, immunologic functions, neurosensory functions, and metabolic functions such as vitamin D synthesis. The skin also provides primary protection against infection by acting as a physical barrier, and when this barrier is damaged pathogens have a direct route to infiltrate the body, possibly resulting in infection.[23] Annually, over 2 million wounds in the United States alone require advanced care; the major etiologies of these complex wounds include venous, diabetic and pressure ulcers, burns, amputations and trauma.[9] Dermatomed, meshed skin grafts, and micrografting of autologous donor skin is efficient for closing large wounds, but results in the creation of additional partial thickness wounds that also need to heal. Alternatively, biological membranes such as cadaver skin, pig skin, and neonatal skin substitutes provide temporary coverage, but are hindered by limited supply and immunological complications.[3] Despite great advances in skin wound care, severe scarring and deformity is one of the greatest challenges facing patients with skin lesions.

The field of tissue engineering and regenerative medicine with its mission to "develop biological substitutes that restore, maintain, or improve tissue function" has been revolutionary in terms of attempting to resolve these shortcomings.[17] Skin tissue regeneration may be achieved through the use of a degradable synthetic membrane on which a patient's

Address correspondence to Nancy A. Monteiro-Riviere, Department of Anatomy and Physiology, Nanotechnology Innovation Center of Kansas State (NICKS), Kansas State University, Manhattan, KS, USA. Electronic mail: nmonteiro@vet.k-state.edu

cells may be seeded. In contrast to conventional grafting, in which autologous donor skin expansion is limited to approximately 1:4 by meshing and micrografting procedures, the rapid growth of patient-derived cells *in vitro* can provide in excess of 60 times the area of the initial biopsy. In this method, cells isolated from patient biopsies as small as 4 square inches can be expanded to cover catastrophic burns covering over 80% of the body in about 2 months.[2] The requirements for suitable tissue engineering scaffolds are demanding and extensive. More specific requirements are necessary on a per tissue basis; for example, skin replacements are required to be bacteriostatic, semi-permeable to water, and cosmetically acceptable.[30] Skin scaffolds should also be elastic enough to withstand cyclic mechanical strains without any significant permanent deformation or creep.[5,14,15]

In the past, tissue scaffolds have been fabricated from synthetic products or from acellular matrices sourced from human tissues. More recently, polymers such as poly(L-lactide) (PLA), poly(glycolic acid) (PGA), poly(ε-caprolactone) (PCL), as well as hydrolyzable and biocompatible copolymers of PLA and PCL (poly(L-lactide-co-epsilon-caprolactone); PLCL) have been used to fabricate successful tissue engineered scaffolds for various soft tissues.[6,7,10,12,16,21] Compared to other bioresorbable polymers such as PGA and PLA, the PLCL copolymer has a slow rate of degradation, with *in vivo* studies reporting 81 mass% retained after 15 weeks of implantation.[14] Scaffolds may be fabricated using an array of different techniques; however, electrospun nanofibrous polymer scaffolds are increasingly being favored since they provide a three-dimensional structure similar to the natural environment and are easily tailored to provide the necessary requirements such as mechanical properties, surface topography and chemistry, and *in vivo* degradation rate.[10,12,20,25] This enables the fabrication of a structure resembling the extracellular matrix with a high surface area to volume ratio.

Infection risks are a danger in any surgical technique, and tissue engineered constructs risk contamination during the *in vitro* culture step and also during implantation. To address this unresolved problem, silver nanoparticles (Ag-nps) have been incorporated into several different medical devices due to their ability to exert antibacterial effects against a both Gram-positive and Gram-negative bacteria, as well as multidrug-resistant strains with limited toxicity.[27,28] Very few Ag-nps electrospun scaffolds have been developed; however, they have taken the approach of loading $AgNO_3$ into the polymer solution and then exposing the scaffold to an annealing process to reduce the precursor into Ag-nps.[13,18] While this process negates complications involving particle agglomeration upon introduction into the polymer solvent, the reduction process can produce a large range in particle sizes and particle attachment location.

The objective of this study was to characterize and assess the biocompatibility of an electrospun scaffold of PLCL nanofibers incorporating antibacterial 20 nm Ag-nps. Since this type of resorbable scaffold has potential applications in the regeneration of skin tissue, this study included an evaluation of the mechanical properties, attachment and proliferation of human epidermal keratinocytes (HEK), the level of antimicrobial activity promoted by the slow release of the silver from the degrading polymer matrix.

MATERIALS AND METHODS

Synthesis and Characterization of Ag-nps

The 20 nm Ag-nps (1.00 mg mL^{-1}) were obtained from NanoComposix (San Diego, CA, USA). Ag-nps were synthesized by ammonium hydroxide catalyzed growth of Ag onto 5 nm gold seed particles while in the presence of citric acid. According to the manufacturer, following synthesis the Ag-nps were concentrated *via* tangential flow filtration, serially washed and suspended in deionized (DI) water and 2 mM citrate buffer. Upon arrival, the Ag-nps were stored at 4 °C in the dark.

Particle size and surface characterization was determined by dynamic light scattering (DLS) and transmission electron microscopy (TEM) to confirm the manufacturer-identified diameters and surface characterization. Ag-nps were suspended at the highest dosing concentration of 100 μg mL^{-1} in deionized (DI) water, Mueller–Hinton bacterial broth, and KGM-2 cell culture medium. Immediately after dispersion, the Ag-nps were placed in a disposable cuvette and DLS measurements were carried out on a Zetasizer Nano-ZS (Malvern Instruments, Inc., Worcestershire, UK). The initial DLS readings were performed at the standard characterization temperature of 25 °C. Each measurement was repeated five times, with 10–20 runs per measurement; data was culled based on the correlogram and size quality report rendered by the Dispersion Technology Software (5.03). Additionally, TEM was utilized to characterize the structure, shape and size uniformity of the Ag-nps. Specimens were prepared by placing 10 μL of homogeneous suspension of Ag-nps at the highest dosing concentration in DI water onto formvar-coated copper mesh grids and air dried. Then, the grids were examined on an FEI/Philips EM 208S TEM operating at an accelerating voltage of 80 kV.

Poly(lactide-co-epsilon-caprolactone) (PLCL) Copolymer

The PLCL copolymer was created using L-lactide (100 mmol), ε-caprolactone (100 mmol), and 1,6-hexanediol (0.5 mmol), which were polymerized at 150 °C for 24 h, using stannous octoate (1 mmol) as a catalyst. After the reaction, the product was dissolved in chloroform and precipitated in methanol, filtered and dried under vacuum. The molar ratio of the two synthetic monomers (PLA and PCL) in the PLCL copolymer was 50:50. The average molecular weight of the copolymer was MW = 350,000. The bulk copolymer was stored in sealed plastic bags in a vacuum desiccator.

Solution Preparation

The solvent used for dissolving the polymer was 1,1,1,3,3,3-hexafluoro-2-propanol (HFIP; Sigma-Aldrich, USA). Based on a previous study performed in our lab,[5] the optimal electrospinning polymer concentration of 11% (w/v) was prepared. Homogeneous solutions were obtained by slow agitation with a magnetic stirrer at 300 rpm for 3 h. The polymer was readily dissolved at room temperature, and the solution remained stable during storage at room temperature for up to 7 days prior to electrospinning. Control polymer solutions were prepared without Ag-nps, and were observed to be clear in appearance.

It was noted that direct addition of Ag-nps into the polymer solution caused particle agglomeration; in order to overcome this problem, prior to Ag-nps addition into the polymer solution, the desired quantity of Ag-nps were first spun down at 16,000 g to form a soft pellet, the water was removed, and the pellet was resuspended into HFIP. Each of the resuspended Ag-nps samples were added to a concentrated polymer solution in order to yield the optimal 11% (w/v) polymer concentration. In this experiment, the Ag-nps samples were added to the polymer solution at a concentration of 0.5 mg Ag-nps (0.5 mL of 1 mg mL^{-1} Ag-nps stock solution, spun down, and water removed) to give a total polymer volume of 15 mL. Using inductively-coupled plasma mass spectroscopy (ICP-MS), the resulting scaffolds were shown to contain 0.11 ± 0.01 mg(Ag) g(scaffold)$^{-1}$. To increase the Ag content of the scaffolds in later experiments, the concentration of the Ag added to the scaffolds was raised by 5 and 10 times the original concentration. The higher concentrations of 0.5 and 1.0 mg Ag-nps (2.5 and 5.0 mL of 1 mg mL^{-1} Ag-nps stock solution, spun down, and water removed) yielded scaffolds with approximately 0.5 and 1.0 mg(Ag) g(scaffold)$^{-1}$. Each polymer solution produced 2 in × 2 in scaffolds ($n = 4$). All scaffolds were sterilized by ethylene oxide prior to use.

Electrospinning

The custom designed electrospinning apparatus consisted of a high-voltage power supply (Gamma High Voltage Research, Inc), an infusion pump (New Era Pump System, Inc), a 15 mL plastic syringe, a stainless steel blunt-ended needle (20 gauge) and a 15 cm diameter metal collector. The syringe was mounted horizontally on the infusion pump and the sample solution was fed at a constant rate through the syringe to the needle tip. The distance between the needle tip and the collector was maintained at 15 cm. The applied voltage to the needle tip was 7.5–10 kV and the flow rate of the solution was 1.0 mL h^{-1}. Control PLCL polymer films were electrospun without Ag-nps. Electrospun scaffolds were collected and the centermost area (4 in × 4 in) was used for all testing.

Fiber Characterization

In order to determine the morphology and diameter of the filaments, the scaffolds were viewed using TEM and scanning electron microscopy (SEM). SEM images were acquired from a JEOL JSM 6360LV SEM using an accelerating voltage of 5 kV. Specimens were mounted on aluminum stubs with conductive carbon tape and then sputter coated with gold/palladium using a Hummer^{TM} 6.2 Sputter Coating System (Anatech, CA, USA) to obtain a conductive coating about 100 Å thick. SEM images of the control and Ag-nps PLCL webs were used to measure the mean fiber diameters. Using ImagePro software, fiber diameters were measured on 100 randomly selected fibers from each individual SEM image. Furthermore, TEM was utilized to confirm the incorporation of Ag-nps within the fibers; copper mesh grids were mounted on the electrospinning collector and the polymer was allowed to spin onto their surface. Grids were then examined on an FEI/Philips EM 208S TEM operating at an accelerating voltage of 80 kV.

Biocompatibility Analysis

Cryopreserved primary neonatal HEK (Lonza, Walkersville, MD) were grown in keratinocyte growth medium-2 (KGM-2; Lonza, Walkersville, MD) in cell culture flasks (75 cm^2; 1,000,000 cells) to approximately 80% confluency in a 37 °C humidified 5% CO$_2$ incubator. Cells were then passed into cell culture plates for biocompatibility testing. For initial toxicity testing of the Ag-nps, HEK were passed into black 96-well microplates (12,500 cells/well; 200 μL) in

which the peripheral wells contained only KGM-2 to prevent the evaporation of treatment medium. Between 18 and 24 h later, after reaching approximately 80% confluency, HEK were exposed for 24 h to either KGM-2 (control) or serial dilutions of Ag-nps starting at 100 μg mL^{-1}. The viability of the HEK was assessed using alamarBlue (aB) viability assay; aB viability assay was used because it was determined to be the best viability assay for examining the toxicity of Ag-nps.[26] The fluorescent values of treated cells were normalized to the control cells, and the data expressed as percentage viability.[22]

For biocompatibility testing of the scaffolds, control and Ag-nps PLCL webs were first soaked in KGM-2 medium overnight prior to cell seeding to facilitate protein adsorption and cell attachment onto the fiber surface. Cells were seeded onto the control and Ag-incorporated scaffolds (1 in $\times$ 1 in) in 6-well plates (50,000 cells per well; 2 mL), and the medium was refreshed every other day. After 7 and 14 days, the aB assay was used to determine cell proliferation within the scaffolding, compared to cells grown as a monolayer in an identical area. Live/Dead viability assay was also used to determine the viability of HEK on the scaffolds and visualize cell attachment, as determined by the percentage of cells that fluoresced green.

Cell attachment and proliferation within the scaffold was also observed using SEM. Images were acquired from a JEOL JSM-6360LV SEM using an accelerating voltage of 5 kV. After cell incubation at 7 and 14 days, scaffolds were fixed with Trump's fixative for 24 h. Then, they were rinsed with 0.1 M phosphate buffer (pH 7.2), followed by deionized water, and then dehydrated by processing through an ascending series of aqueous ethanol solutions. The scaffolds were then submersed in hexamethyldisilazane overnight, sputter coated as described above, and then observed by SEM.

Degradation

Papain enzyme was used to simulate an accelerated *in vivo* enzymatic environment.[5,20] The papain enzyme solution was activated prior to the start of the degradation study by adding 0.01 M EDTA solution with 0.05 M of cysteine, papain from papaya latex (Sigma Aldrich, USA), 0.01 M ethylenediaminetetraacetic acid (EDTA) (Sigma Aldrich, USA), and 0.05 M L-cysteine hydrochloride monohydrate (Sigma Aldrich, USA). The activated solution was prepared based on the mole ratio of 1: 2.5: 12.5 between enzyme, EDTA, and cysteine respectively. In order to maintain the activity of the enzyme during the entire degradation period, the enzyme solutions were replenished with activated enzymes after every 72 h. Scaffolds (1 in $\times$ 1 in) were subjected to the degradation

solution for 7 days at 37 °C. The mass of dry scaffolds was measured before and after the degradation treatment. Additionally, ICP-MS was used to confirm the linearity of Ag release during scaffold degradation.

Antibacterial Efficacy

Cation-adjusted Mueller–Hinton (MH) broth and agar (Difco Laboratories, Detroit, MI) was used as the bacterial cultivating medium for *Escherichia coli* MG1655 and *Staphylococcus aureus* (ATCC 25213). Isolated bacterial colonies were grown overnight at 37 °C from frozen samples on an agar plate. The broth microdilution minimum inhibitory concentration (MIC) test was conducted to measure the *in vitro* activity of Ag-nps against each bacterial isolate.[29] Briefly, a sterile round-bottom plastic 96-well plate was loaded with 100 μL of serially 1:2 diluted concentrations of Ag-nps. Ag-nps samples were tested at ten serially diluted concentrations starting at the highest dosing concentration that their supplied concentrations would allow (1.00 mg mL^{-1}). Silver nitrate (AgNO$_3$; 99.9%, Sigma-Aldrich, St. Louis, MO) was used as the positive control source of Ag$^+$ ions. For each bacterial strain, a bacterial colony was suspended into phosphate buffered saline (PBS) to 0.5 McFarland (10^8 CFU/mL), diluted 1:20 into MH broth, and added into the treatment wells at 100 μL of 5–8 $\times$ 10^5 CFU/mL ($n = 8$ wells/treatment). To ensure quality control and for seeding accuracy, inoculating bacteria were diluted in PBS at 10^3, 10^4, 10^5, and 10^6 and plated overnight. Microplates were incubated at 37 °C and shaken at 200 rpm for 24 h. After the microplates were incubated for 24 h at 37 °C, the lowest concentration showing no visible growth was recorded as the MIC. To determine the MBC, 10 μL from all of the clear wells (MIC and higher concentrations) was dropped onto a MH agar plate and incubated for 24 h at 37 °C. The minimum bactericidal concentration (MBC) was determined by the concentration that failed to yield growth.

To assess the antibacterial efficacy of the Ag incorporated scaffolds, 100 μL of the degradation solution from each scaffold was plated onto bacterial lawns and allowed to grow overnight. To prevent agar degradation, the degradation solution was briefly heated to 100 °C to inactivate remaining papain and then cooled prior to plating. Any bacterial inhibition caused by the released Ag was recorded.

Tensile Testing

The mechanical properties of the PLCL scaffolds was assessed *via* uniaxial tensile testing to failure at a cross-head speed of 0.5 mm/s, during which force and

displacement data as well as videos were recorded, as well as video recording of the gauge length over time ($n = 4$ for each group). All specimens were prepared by punching into dog-bone shaped specimens using a die with a gauge length of 20 and 5 mm. Naked scaffolds were tested "as is," while 14 days cell growth scaffolds and 7 days degraded scaffolds were transferred directly from their cell culture plates to a board where they were lightly blotted, punched, and immediately tested. Specimens were mounted between pneumatic grips with a 250 g load cell mounted under the bottom fixed grip. Acellular and 14 days cell growth control scaffolds were tested using an ElectroForce (Bose, Minnesota, USA) mechanical system, but malfunction of the system required all other specimens to be tested using a Mini-Bionix II mechanical testing machine (MTS, Minnesota, USA). The load cell and all other test conditions were maintained. The modulus of elasticity was calculated from the slope of the linear portion of the standard stress–strain curves. The strain was calculated from the recorded videos using ImagePro software to track the movement of dots drawn onto the scaffold gauge length.

Statistical Analysis

The mean values for fiber diameter, HEK percent viability (Live/Dead assay), and MIC/MBC values were calculated, and the significant differences between the means ($p < 0.05$) were determined by the PROC GLM Procedure (SAS 9.1 for Windows; SAS Institute, Cary, NC); significant differences between the mean values for proliferation (aB assay; normalized to control cells grown as a monolayer) and modulus of elasticity were analyzed by two-way ANOVA with respect to Ag content and cellular or degradation treatment. For all analyses, when significant differences were found, multiple comparisons were performed using Tukey's Studentized Range High Standard Deviation test at $p < 0.05$ level of significance. The data were expressed as the mean ± standard error of the mean (SEM) for $n = 6$.

RESULTS

Cytotoxicity

As the concentration of the 20 nm Ag-nps increased, there was no significant decrease in HEK viability following 24 h exposure until 50 μg mL^{-1}, and at 100 μg mL^{-1} there was nearly a complete loss of viability (Fig. 1).

Fiber and Ag-nps Morphology

The physicochemical properties of the 20 nm Ag-nps can be found in Table 1, which lists their physical and hydrodynamic diameters according to TEM and DLS, respectively, as well as the supplied Ag-nps solution concentration, particle concentration, and zeta potential. As is typical for nanoparticles, the hydrodynamic diameter of the 20 nm Ag-nps measured by DLS was slightly larger (27.4 nm) than the physical diameter measured by TEM (19.2 nm). The significantly larger hydrodynamic diameter is most likely attributable to the formation of small, loosely bound Ag-nps dimers. Agglomeration of Ag-nps occurred after incorporation into MH broth (659.3 ± 30.7) and KGM-2 medium (2721.5 ± 178.3) which is consistent with the previously reported behavior of nanoparticles which are known to physically interact with proteins and promote agglomeration.[22,23,26] The zeta potential of a colloid suspension characterizes its stability and ability to resist aggregation, with greater zeta potentials having greater stability. The 20 nm Ag-nps suspension had a zeta-potential
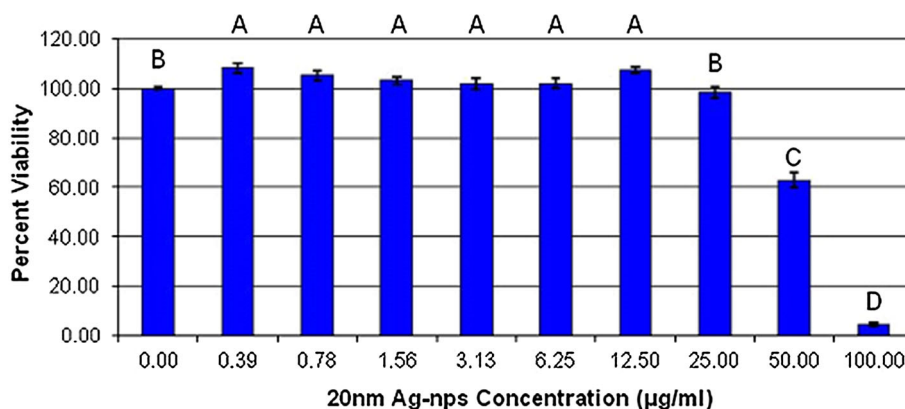

FIGURE 1. HEK viability after 24 h exposure to 20 nm Ag-nps. Different letters denote statistical significance ($p < 0.05$) between concentrations.

of -50 eV which indicates good stability due most likely to the stabilizing effect of the citrate buffer. Based on TEM evaluation, the 20 nm Ag-nps were spherical in shape and highly uniform in size both before and after incorporation into the PLCL fibers (Figs. 2a–2d). It was noted that at the lowest concentration of incorporation that small agglomerates were interspersed throughout the fibers (Fig. 2b), at 0.5 mg(Ag) g(scaffold)$^{-1}$ the Ag-nps were highly monodisperse (Fig. 2c), and at the highest concentration the Ag-nps appeared to align within the fibers (Fig. 2d).

By visual observation, control PLCL scaffold appeared white whereas Ag-np incorporated PLCL scaffolds appeared increasingly grey with increasing concentration. The morphology of the obtained PLCL fibers was observed using SEM. Figures 3a–3l show selected SEM images of control and Ag-nps PLCL webs before and after HEK cell culture for 7 and 14 days. Smooth, connected fibers were observed in Figs. 3c, 3d, 3h and 3l as well as fiber agglomeration in Figs. 3a, 3b, 3e and 3f, which is indicative of incomplete solvent evaporation. No significant difference in

TABLE 1. Physicochemical properties of Ag-nps.

MDD (nm)	DLS diameter (nm)[a]	DLS diameter (nm)[b]	DLS diameter (nm)[c]	TEM diameter (nm)	Supplied Conc. (mg mL^{-1})	Particle Conc. (particles mL^{-1})	Zeta[a] diameter (mV)
20	27.4 ± 0.2	2721.5 ± 178.3	659.3 ± 30.7	19.2 ± 2.2	1.00	2.6 × 10^{13}	−49.8 ± 0.5

Data are expressed as mean ± standard error of the mean; [a] DI water, [b] KGM-2 medium, [c] MH broth; MDD, manufacturer-designated diameter; DLS, dynamic light scattering; TEM, transmission electron microscopy.
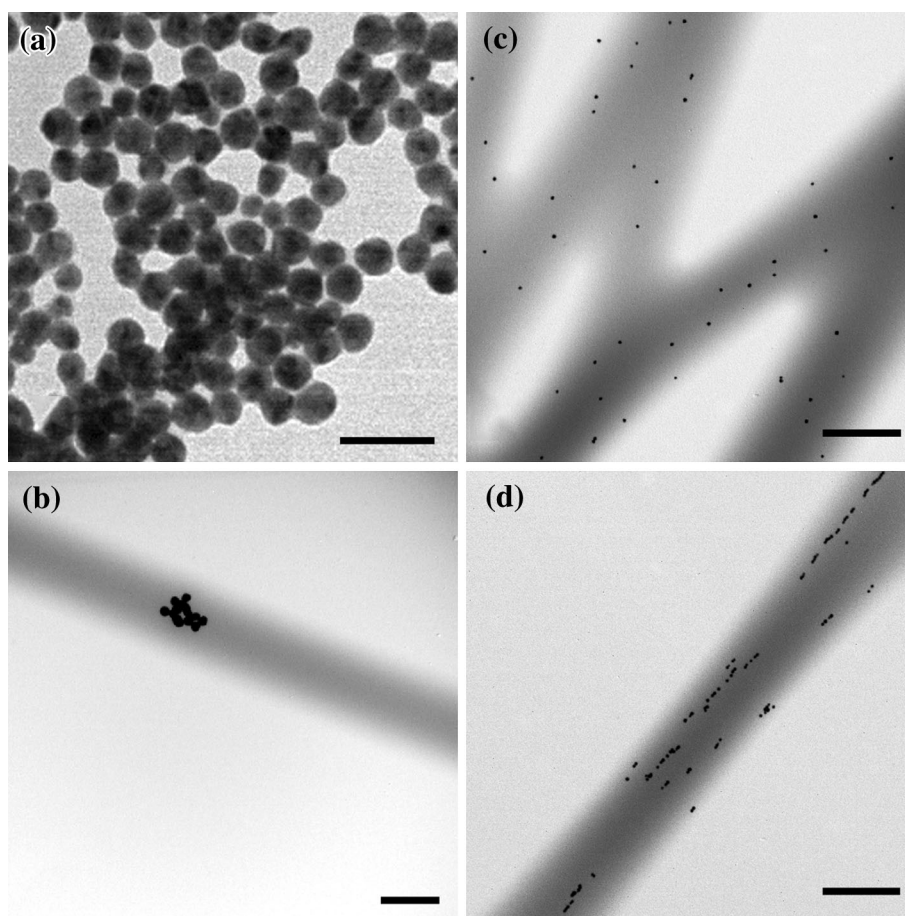

FIGURE 2. Transmission electron micrographs of Ag-nps and Ag-nps incorporated PLCL scaffolds. (a) 20 nm Ag-nps, Bar = 50 nm; (b) 0.1 mg(Ag) g(scaffold)$^{-1}$, Bar = 0.5 μm; (c) 0.5 mg(Ag) g(scaffold)$^{-1}$, Bar = 0.5 μm; (d) 1.0 mg(Ag) g(scaffold)$^{-1}$, Bar = 0.5 μm.
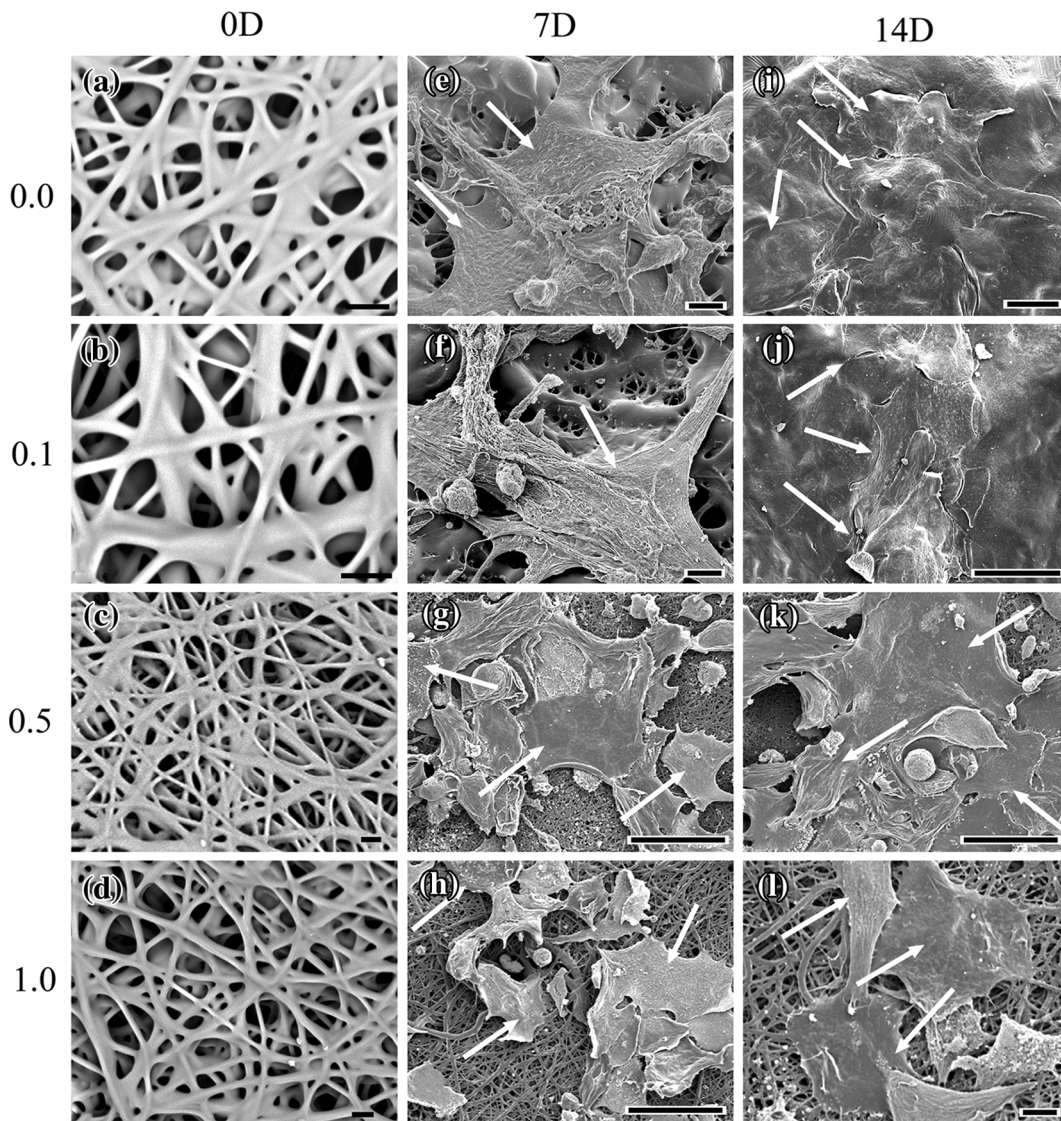
FIGURE 3. Scanning electron micrographs of PLCL webs before and after 7 and 14 days growth of HEK. (a) 0.0 mg(Ag) g(scaffold)$^{-1}$ PLCL, 0 days, Bar = 10 μm; (b) 0.1 mg(Ag) g(scaffold)$^{-1}$, 0 days, Bar = 10 μm; (c) 0.5 mg(Ag) g(scaffold)$^{-1}$, 0 days, Bar = 10 μm; (d) 1.0 mg(Ag) g(scaffold)$^{-1}$, 0 days, Bar = 10 μm; (e) 0.0 mg(Ag) g(scaffold)$^{-1}$, 7 days, Bar = 10 μm; (f) 0.1 mg(Ag) g(scaffold)$^{-1}$, 7 days, Bar = 10 μm; (g) 0.5 mg(Ag) g(scaffold)$^{-1}$, 7 days, Bar = 50 μm; (h) 1.0 mg(Ag) g(scaffold)$^{-1}$, 7 days, Bar = 50 μm; (i) 0.0 mg(Ag) g(scaffold)$^{-1}$, 14 days, Bar = 20 μm; (j) 0.1 mg(Ag) g(scaffold)$^{-1}$, 14 days, Bar = 10 μm; (k) 0.5 mg(Ag) g(scaffold)$^{-1}$, 14 days, Bar = 50 μm; (l) 1.0 mg(Ag) g(scaffold)$^{-1}$, 14 days, Bar = 50 μm. Arrows denote HEK cells.

average fiber diameters ($p < 0.05$) was noted between the control, 0.1 and 0.5 mg Ag/g scaffolds; the average diameter for the control PLCL web was 2.25 μm $\pm$ 0.18 μm, while the average fiber diameter for the 0.1 and 0.5 mg Ag/g scaffold webs were 2.70 μm $\pm$ 0.19 μm and 2.54 μm $\pm$ 0.78 μm, respectively. However, the 1.0 mg Ag/g scaffold web had a significantly increased ($p < 0.05$) average diameter of 3.96 μm $\pm$ 0.36 μm.

Biocompatibility

SEM images depicted the attachment and proliferation of HEK on both control and Ag-nps PLCL samples throughout their 7 and 14 days time period of cell culture, exhibiting characteristic HEK morphology (Figs. 3e–3l). Following 7 days of incubation, individual HEK were easily observed on both the control and each of the Ag-np incorporated PLCL webs

(Figs. 3e–3h). After 14 days, the HEK were able to form confluent monolayers on both the control and 0.1 mg(Ag) g(scaffold)$^{-1}$ webs (Figs. 3i and 3j, respectively). As the concentration of Ag within the PLCL scaffold was increased, the attachment of HEK was observably decreased after 7 days (Figs. 3g, 3h) as well as their ability to achieve confluency over the surface of the scaffolds (Figs. 3k, 3l).

To analyze whether the cells in the scaffolds remained viable after 7 and 14 days, a Live/Dead cell viability assay was used. No significant decreases in cell viability were noted at either time point for the control

or 0.1 mg Ag/g scaffold webs (Figs. 4a, 4b, 4e, 4f). As shown, nearly all of the cells were viable 7 and 14 days on both control (Figs. 4a, 4e) and 0.1 mg(Ag) g(scaffold)$^{-1}$ webs (Figs. 4b, 4f). For the 0.5 mg(Ag) g(scaffolds)$^{-1}$ webs (Figs. 4c, 4g), the presence of dead cells is readily apparent after 14 days. Moreover, a decrease in HEK viability was observed by the presence of dead cells after 7 and 14 days growth for the 1.0 mg(Ag) g(scaffold)$^{-1}$ webs (Figs. 4d, 4h) ($p < 0.05$). Additionally for each of the webs, some cells appear out of focus, confirming cell infiltration into the scaffold interior.

The HEK proliferation was confirmed using aB viability assay, and the results are presented in Table 2. Two-way ANOVA with *post hoc* analysis revealed significant differences between scaffolds ($p < 0.05$) for both time points. Compared to cells grown as a monolayer, HEK proliferation was observed to increase to approximately 120% by 7 days and over 200% by 14 days on control PLCL scaffolds. Similar to the observation of decreased HEK attachment following an increase in Ag concentration, an increase in Ag content resulted in a decrease in HEK viability (Table 2). For the 0.1, 0.5, and 1.0 mg(Ag) g(scaffolds)$^{-1}$ the proliferation of HEK was approximately 110, 100, and 75% for 7 days, respectively, and 210, 150, and 100% by 14 days, respectively. Despite the decreasing trend, the greater than 100% proliferation is indicative of HEK growth along the increased surface area provided by the three-dimensional structure of the webs, compared to monolayer growth.

Mechanical Properties

The addition of Ag-nps altered the mechanical properties of the PLCL scaffold at 14 days of cell culture and 7 days of *in vitro* enzymatic degradation (Fig. 5). Uniaxial tensile tests of the PLCL scaffolds revealed a statistically significant ($p < 0.001$) decrease in the modulus of elasticity (E) values for 0.1 mg(Ag) g(scaffold)$^{-1}$ webs (1.14 MPa), 0.5 mg(Ag) g(scaffold)$^{-1}$ webs (1.08 MPa), and 1.0 mg(Ag) g(scaffold)$^{-1}$ webs (1.03 MPa) compared to the PLCL control (1.78 MPa) for all treatments. Growth of cells on the scaffolds for 14 days was shown to significantly increase ($p < 0.001$) E for each of the PLCL scaffolds (1.66, 1.53, and 1.27 MPa for the 0.1, 0.5, and 1.0 mg(Ag) g(scaffold)$^{-1}$ webs, respectively, compared to the acellular treatment group. Not surprisingly, *in vitro* enzymatic degradation of the scaffolds was associated with a statistically significant ($p < 0.001$) decrease in the modulus of elasticity for each of the 0.1, 0.5 and 1.0 mg(Ag) g(scaffolds)$^{-1}$ (0.94, 0.88, 0.83 MPa, respectively), compared to the 0.0 mg(Ag) g(scaffolds)$^{-1}$ (1.45 MPa).
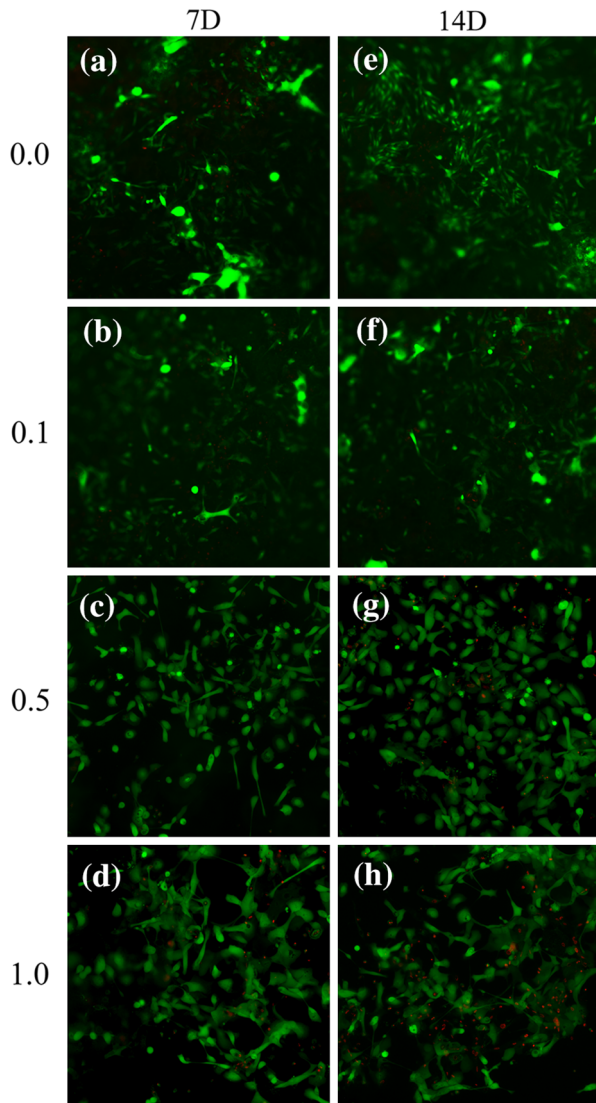

FIGURE 4. Fluorescent images of HEK after 7 and 14 days on PLCL scaffolds, proliferation assessed using Live/Dead assay. (a) 0 mg(Ag) g(scaffold)$^{-1}$, 7 days; (b) 0.1 mg(Ag) g(scaffold)$^{-1}$, 7 days; (c) 0.5 mg(Ag) g(scaffold)$^{-1}$, 7 days; (d) 1.0 mg(Ag) g(scaffold)$^{-1}$, 7 days; (e) 0.0 mg(Ag) g(scaffold)$^{-1}$, 14 days; (f) 0.1 mg(Ag) g(scaffold)$^{-1}$, 14 days; (g) 0.5 mg(Ag) g(scaffold)$^{-1}$, 14 days; (h) 1.0 mg(Ag) g(scaffold)$^{-1}$, 14 days. Live cells stain green and dead cells stain red. Magnification of 10× for all images.

TABLE 2. HEK Proliferation on PLCL Scaffolds.

	Percent viability compared to monolayer growth	
	Time point	
Scaffold type	7 days	14 days
0.0 mg(Ag) g^{-1} 50:50 PLCL scaffold	124.5 ± 0.5	223.1 ± 1.4
0.1 mg(Ag) g^{-1} 50:50 PLCL scaffold	112.6 ± 0.4	213.9 ± 2.7
0.5 mg(Ag) g^{-1} 50:50 PLCL scaffold	98.3 ± 1.8	150.2 ± 5.2
1.0 mg(Ag) g^{-1} 50:50 PLCL scaffold	75.9 ± 2.4	102.0 ± 1.1

All data is expressed as mean ± standard error of the mean. Two-way ANOVA with *post hoc* analysis revealed significant differences between each scaffold ($p < 0.05$) for both time points.
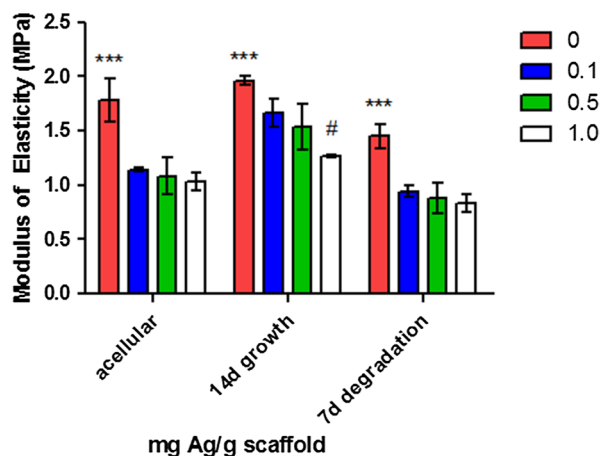

FIGURE 5. Modulus of elasticity (E) for PLCL scaffolds under uniaxial tensile stress. All data is expressed as mean ± standard error of the mean (MPa). * Denotes statistical difference ($p < 0.001$) between 0 mg(Ag) g(scaffold)$^{-1}$ and all other scaffolds for each treatment set; # denotes additional statistical difference ($p < 0.001$) between 1.0 mg(Ag) g(scaffold)$^{-1}$ and all other scaffolds for 14 days cellular growth treatments.

Antibacterial Efficacy

The 20 nm Ag-nps alone were shown to inhibit the growth of *S. aureus* and *E. coli* MG1655. The MIC and MBC values for each strain were found to be 32.0 and 32.0 μg mL^{-1} for *S. aureus*, whereas the MIC and MBC was 64.0 and 85.3 μg mL^{-1} for *E. coli* (Table 3). The control and 0.1 mg(Ag) g(scaffolds)$^{-1}$ were not shown to inhibit bacterial growth, while the 0.5 and 1.0(Ag) g(scaffolds)$^{-1}$ were shown to minimally and substantially inhibit the growth of both bacterial strains (Figs. 6a, 6b). Exposure to *in vitro* enzymatic degradation was performed to mimic accelerated *in vivo* degradation and allow for the release of antimicrobial Ag-nps and Ag ions. Degradation for 7 days caused a loss in mass of 40.9% for the control PLCL scaffold, compared to 37.6, 39.1, and 36.9% for the 0.1, 0.5, and 1.0 mg(Ag) g(scaffolds)$^{-1}$, respectively.

ICP-MS analysis showed that the Ag content in the scaffolds before and after degradation treatment remained constant, implying uniform degradation of the scaffolds and release of Ag-nps. Following 7 days degradation, the Ag content of the 0.1, 0.5, and 1.0 mg(Ag) g(scaffolds)$^{-1}$ scaffolds was 0.11 ± 0.02, 0.49 ± 0.02, and 1.11 ± 0.00 mg(Ag) g(scaffold)$^{-1}$, respectively. However, the amount of Ag-nps released from the PLCL scaffold into the KGM-2 medium or the enzymatic degradation solution was sufficient only at the highest concentration of 1.0 mg(Ag) g(scaffolds)$^{-1}$ to impart antibacterial efficacy against either of the bacterial strains tested.

DISCUSSION

In recent years, interest has grown for the utilization of Ag-nps rather than traditional antibiotics due to their broad antimicrobial activity against both Gram-negative and Gram-positive bacteria, including multi-drug-resistant strains.[27,28] The application of Ag-nps in tissue engineered scaffolds for skin regeneration is pivotal in the reduction of infection that is rampant particularly in burn wounds. Many successful and promising attempts have been made to incorporate Ag-nps into biomaterials for continuous release to impart antibacterial activity including nanoparticulate Ag bone cement[1] and titanium implants coated with a silver-hydroxyapatite layer.[4] Attempts have also been made to investigate the feasibility of the incorporation of Ag-nps into polymer scaffolds for various antimicrobial applications.[8,11]

However, before the scaffold is used for *in vivo* tissue engineering, it is essential to identify an optimum concentration of released Ag-nps that would show antimicrobial activity without having any cytotoxic effect on the cells of the targeted tissue. Additionally, it has been reported that Ag-nps of various sizes can cause toxicity to various human cell lines *in vitro*, and it was therefore important to limit the concentration of the Ag-nps incorporated into PLCL scaffolds in this study.[19,24]

The present study highlights the usefulness of incorporating 20 nm Ag-nps into electrospun PLCL scaffolds in order to both foster the growth of HEK, and to ideally impart some level of antimicrobial activity through the protracted release of Ag-nps into the culture medium. This was achieved through the fabrication of PLCL scaffolds that incorporated Ag-nps, and was based upon the established electrospinning parameters developed in our laboratory.[5] It was confirmed by TEM that the 20 nm Ag-nps were well incorporated within the fibers. While HEK exposed to the 20 nm Ag-nps alone caused a significant

TABLE 3. Minimal inhibitory concentrations (MIC) and minimal bactericidal concentrations (MBC).

	AgNO$_3$		20 nm Ag-nps	
Bacterial strain	MIC (μg/mL)	MBC (μg/mL)	MIC (μg/mL)	MBC (μg/mL)
S. aureus	2	4	32	32
E. coli	2	2	64	85.3

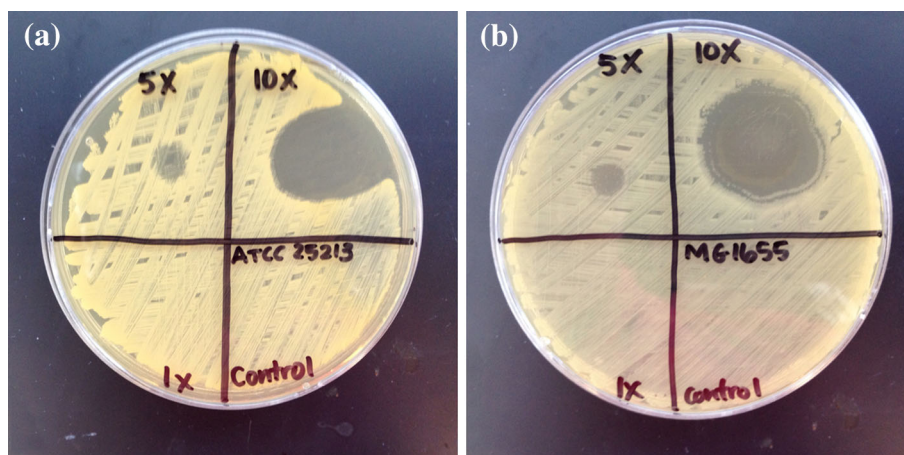The data are expressed as means. All standard errors of the means were zero.

FIGURE 6. Antibacterial efficacy of PLCL scaffolds incorporated with 0.0 ("0"), 0.1 ("1×"), 0.5 ("5×"), and 1.0 ("10×") mg(Ag) g(scaffold)$^{-1}$. (a) *Staphylococcus aureus* (ATCC 25213), (b) *Escherichia coli* (MG1655).

decrease in viability starting at 50 μg mL^{-1}, their incorporation into the PLCL scaffold only resulted in a substantial decrease in cell viability for the highest Ag concentration of 1.0 mg(Ag) g(scaffolds)$^{-1}$ webs. In fact, the HEK flourished on and within the majority of the scaffolds after 7 and 14 days of culture. The morphologic observations of cell behavior on the nanofiber scaffolds confirmed that HEK proliferated well on the Ag-nps containing nanofibers as monolayer cultures. Additionally, the range in modulus of elasticity of 0.83–1.78 MPa for the Ag-nps containing PLCL scaffolds compares well to that found by an electrospun PLCL scaffold of similar dimensions by others (0.8 MPa).[16]

The antibacterial results for the 20 nm Ag-nps alone are congruent with our previous studies for 20 nm Ag-nps stabilized in a phosphate buffer.[27] An initial antibacterial efficacy test of Ag-np incorporated scaffolds was performed by placing uniform disks of each scaffold onto bacterial lawns and into bacterial broths. It was observed that the scaffold could not deliver overnight or 24 h inhibition of bacterial growth, likely due to the slow release of Ag from the scaffolds over time. Therefore, enzymatic degradation of the scaffolds was conducted in order to simulate the protracted release of Ag. Based on the

bacterial inhibition results of released Ag, it can be concluded that at least a 0.5 mg(Ag) g(scaffolds)$^{-1}$ is necessary to inhibit both Gram-positive and Gram-negative bacterial growth. However, this result also highlights the necessity for combination therapies, in order to deliver an immediate antimicrobial to the wound site. A potential method could employ a coating of Ag-nps onto the scaffold surface at a concentration less than 100 μg mL^{-1} (Table 3).

This study sought to use electrospinning to fabricate a novel antibacterial skin scaffolding material composed of PLCL degradable copolymer incorporated with Ag-nps. The potential use of the electrospun Ag-nps PLCL scaffold for skin regeneration was evaluated *in vitro* with HEK using models for cell attachment, proliferation and viability, with Gram-positive and Gram-negative bacterial strains for antibacterial efficacy, and a uniaxial tensile test for biomaterial mechanical properties. In conclusion, PLCL is a suitable choice for soft tissue scaffolds since it is biocompatible, facilitates rapid attachment and growth of cells, and has a low modulus of elasticity similar to that of human skin. These results showed that the release of Ag content was sufficient to inhibit bacterial growth at a scaffold concentration between 0.5 and 1.0 mg(Ag) g(scaffolds)$^{-1}$. Additionally, these scaffolds supported the robust attachment and proliferation of keratinocytes

on the scaffold, while maintaining sufficient mechanical properties to warrant skin implantation.

ACKNOWLEDGMENTS

REFERENCES

[1]Alt, V., T. Bechert, P. Steinrücke, M. Wagener, P. Seidel, E. Dingeldein, E. Domann, and R. Schnettler. An in vitro assessment of the antibacterial properties and cytotoxicity of nanoparticulate silver bone cement. *Biomaterials* 18:4383–4391, 2004.

[2]Boyce, S. T., R. J. Kagan, D. G. Greenhalgh, P. Warner, K. P. Yakuboff, T. Palmieri, and G. D. Warden. Cultured skin substitutes reduce requirements for harvesting of skin autograft for closure of excised, full-thickness burn. *J. Trauma.* 60(4):821–829, 2006.

[3]Burd, A., and T. Chiu. Allogenic skin in the treatment of burns. *Clin. Dermatol.* 23:376–387, 2005.

[4]Chen, W., Y. Liu, H. S. Courtney, M. Bettenga, C. M. Agrawal, D. Bumgardner, and J. L. Ong. In vitro antibacterial and biological properties of magnetron co-sputtered silver-containing hydroxyapatite coating. *Biomaterials* 27:5512–5517, 2006.

[5]Chung, S., N. P. Ingle, G. A. Montero, S. H. Kim, and M. W. King. Bioresorbable elastomeric vascular tissue engineering scaffolds via melt spinning and electrospinning. *Acta Biomater.* 6(6):1958–1967, 2010.

[6]De Groot, J. H., F. M. Zijlstra, H. W. Kuipers, A. J. Pennings, J. Klompmaker, R. P. H. Veth, and H. W. Jansen. Meniscal tissue regeneration in porous 50/50 co-poly(L-lactide/ε-caprolactone) implants. *Biomaterials* 18(8):613–622, 1997.

[7]Den Dunnen, W. F., B. van der Lei, P. H. Robinson, A. Holwerda, A. J. Pennings, and J. M. Schakenraad. Biological performance of a degradable poly(lactic acid-ε-caprolactone) nerve guide influence of tube dimensions. *J. Biomed. Mater. Res.* 29(6):757–766, 1995.

[8]Furno, F., K. S. Morley, B. Wong, B. L. Sharp, P. L. Arnold, S. M. Howdle, R. Bayston, P. D. Brown, P. D. Winship, and H. J. Reid. Silver nanoparticles and polymeric medical devices: a new approach to prevention of infection? *J. Antimicrob. Chemother.* 54:1019–1024, 2004.

[9]Garfein, E. Skin replacement products and markets. In: Biomaterials for Treating Skin Loss. Boca Raton, FL: CRC Press, 2009, pp. 9–17.

[10]Hiljanen-Vainio, M., T. Karjalainen, and J. Seppala. Biodegradable lactone copolymers. 1. Characterization and mechanical behavior of ε-caprolactone and lactide copolymers. *J. Appl. Polym. Sci.* 59(8):1281–1288, 1996.

[11]Hong, K. H., J. L. Y. Park, I. H. Sul, J. H. Youk, and T. J. Kang. Preparation of antimicrobial poly(vinyl alcohol) nanofibers containing silver nanoparticles. *J. Polym. Sci. Part B* 44(17):2468–2474, 2006.

[12]Inoguchi, H., I. K. Kwon, E. Inoue, K. Takamizawa, Y. Maehara, and T. Matsuda. Mechanical responses of a compliant electrospun poly(L-lactide-co-epsilon-caprolactone) small-diameter vascular graft. *Biomaterials* 27:1470–1478, 2006.

[13]Jeon, H. J., J. S. Kim, T. G. Kim, J. H. Kim, W.-R. Yu, and J. H. Youk. Preparation of poly(ε-caprolactone)-based polyurethane nanofibers containing silver nanoparticles. *Appl. Surf. Sci.* 254(18):5886–5890, 2008.

[14]Jeong, S. I., S. H. Kim, Y. H. Kim, Y. Jung, J. H. Kwon, B. S. Kim, and Y. M Lee. Manufacture of elastic biodegradable PLCL scaffolds for mechano-active vascular tissue-engineering. *J. Biomater. Sci. Polym. Ed.* 15(5):645–660, 2004.

[15]Kim, B.-S., and D. J. Mooney. Scaffold for engineering smooth muscle under cyclic mechanical strain conditions. *J. Biomech. Eng.* 122:210–215, 2000.

[16]Kwon, K., S. Kidoaki, and T. Matsuda. Electrospun nano-to microfiber fabrics made of biodegradable copolyesters: structural characteristics, mechanical properties and cell adhesion potential. *Biomaterials* 26(18):3929–3939, 2005.

[17]Langer, R., and J. P. Vacanti. Tissue engineering. *Science* 260(5110):920–928, 1993.

[18]Liu, X., T. Lin, J. Fang, G. Yao, H. Zhao, M. Dodson, and X. Wang. In vivo wound healing and antibacterial performances of electrospun nanofiber membranes. *J. Biomed. Mater. Res. A* 94(2):499–508, 2010.

[19]Liu, W., Y. Wu, C. Wang, H. C. Li, T. Wang, C. Y. Liao, L. Cui, Q. F. Zhou, B. Yan, and G. B. Jiang. Impact of silver nanoparticles on human cells: effect of particle size. *Nanotoxicol.* 4(3):319–330, 2010.

[20]McCullen, S. D., D. R. Stevens, W. A. Roberts, L. I. Clarke, S. H. Bernacki, R. E. Gorga, and E. G. Loboa. Characterization of electrospun nanocomposite scaffolds and biocompatibility with adipose-derived human mesenchymal stem cells. *Int. J. Nanomedicine* 2(2):253–263, 2007.

[21]Mo, X. M., C. Y. Xu, M. Kotaki, and S. Ramakrishna. Electrospun P(LLA-CL) nanofiber: a biomimetic extracellular matrix for smooth muscle cell and endothelial cell proliferation. *Biomaterials* 25(10):1883–1890, 2004.

[22]Monteiro-Riviere, N. A., A. O. Inman, and L. W. Zhang. Limitations and relative utility of screening assays to assess engineered nanoparticle toxicity in a human cell line. *Tox. Appl. Pharma.* 234:222–235, 2009.

[23]Monteiro-Riviere, N. A. Structure and function of skin. In: Toxicology of the Skin-Target Organ Series, edited by N. A. Monteiro-Riviere. New York: Informa Healthcare, 2010, Vol. 29, pp. 1–18.

[24]Park, E.-J., J. Yi, Y. Kim, K. Choi, and K. Parl. Silver nanoparticles induce cytotoxicity by a Trojan-horse type mechanism. *Toxicol. In Vitro* 24(3):872–878, 2010.

[25]Pham, Q. P., U. Sharma, and A. G. Mikos. Electrospinning of polymeric nanofibers for tissue engineering applications: a review. *Tissue Eng.* 12(5):1197–1211, 2006.

[26]Samberg, M. E., S. J. Oldenburg, and N. A. Monteiro-Riviere. Evaluation of silver nanoparticle toxicity in skin in vivo and keratinocytes in vitro. *Environ. Health Perspect.* 118(3):407–413, 2010.

[27]Samberg, M. E., P. E. Orndorff, and N. A. Monteiro-Riviere. Antibacterial efficacy of silver nanoparticles of

different sizes, surface conditions and synthesis methods. *Nanotoxicology* 5(2):244–253, 2011.

[28]Shahverdi, A. R., A. Fakhimi, H. R. H. R. Shahverdi, and S. Minaian. Synthesis and effect of silver nanoparticles on the antibacterial activity of different antibiotics against Staphylococcus aureus and Escherichia coli. *Nanomedicine* 3(2):168–171, 2007.

[29]Wikler, M. A., F. R. Cockerill III, K. Bush, M. N. Dudley, G. E. Eliopoulos, D. J. Hardy, *et al.* Methods for dilution antimicrobial susceptibility tests for bacteria that grow aerobically. In: Approved Standard-8th Edition, Clinical and Laboratory Standards Institute Document M07-A8. Wayne, PA, 2009, 29(2).

[30]Zhong, S. P., Y. Z. Zhang, and C. T. Lim. Tissue scaffolds for skin wound healing and dermal reconstruction. *WIREs Nanomed. Nanobiotechnol.* 2:510–525, 2010.